Figure S1- related to main Figure 1

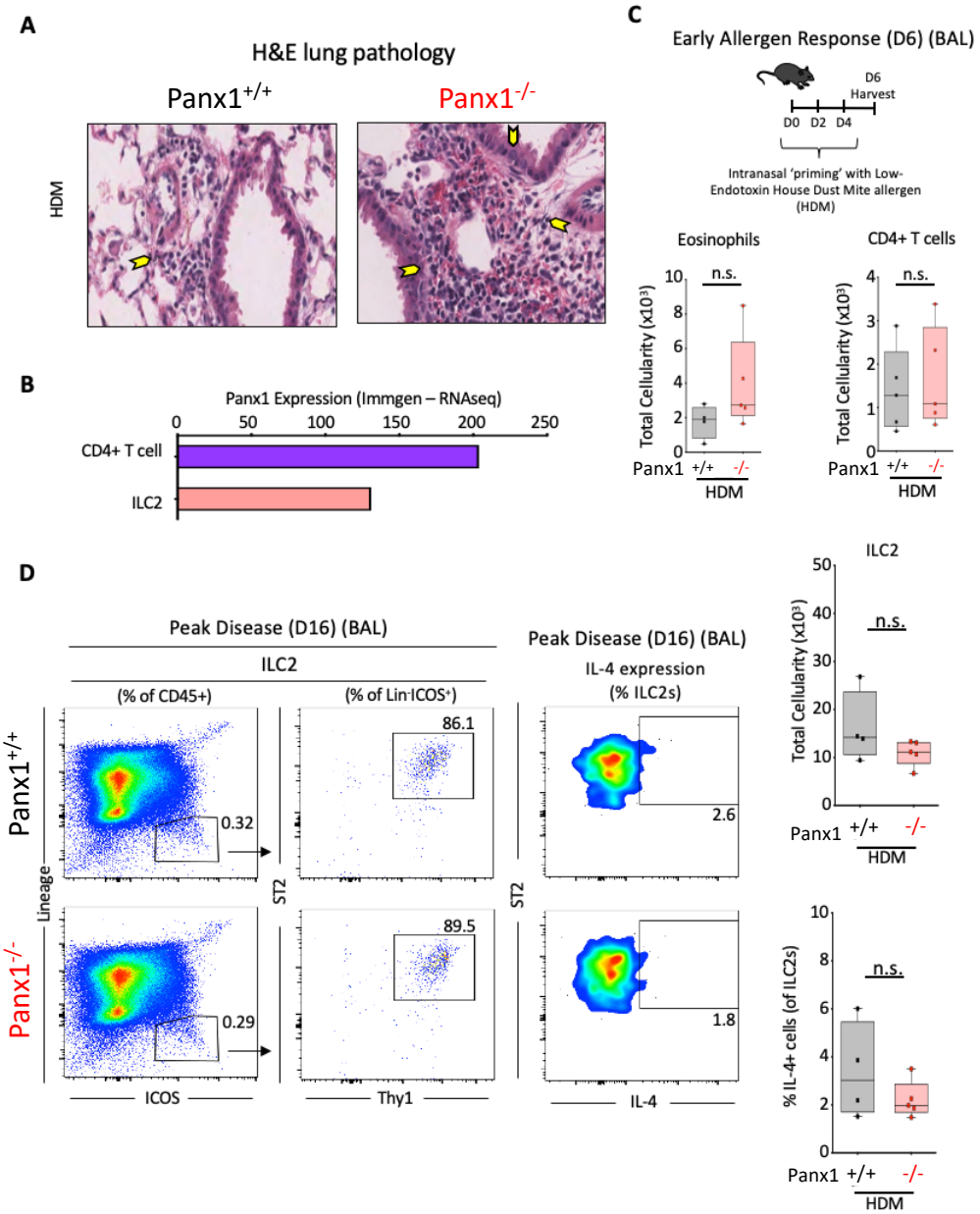

Figure S1, related to main Figure 1. *Panx1*$^{-/-}$ mice exhibit increased histological disease severity at peak disease, but do not show increase in ILC2s.

(A) Magnified H&E lung histology images of wild-type and global *Panx1*$^{-/-}$ mice from Figure 1C during HDM challenge. Arrows highlight areas of immune cell infiltration and inflammation.

(B) Gene expression data from the Immgen database assessing the relative expression of *Panx1* across several immune cell types.

(C) Schematic representation of house dust mite (HDM)-induced allergic airway inflammation for focusing on the innate immune response (top). Absolute cellularity of eosinophils and CD4^{+} T cells in wild type or *Panx1*$^{-/-}$ mice after HDM challenge (bottom) (*Panx1*$^{+/+}$ *n=4-5, Panx1*$^{-/-}$ *n=5*). Unpaired Student's t-test.

(D) Flow plots showing ILC2 infiltration and percentage of IL4^{+} ILC2s into the lung at peak disease after HDM challenge (left) and quantification (right) (*Panx1*$^{+/+}$ *n=4, Panx1*$^{-/-}$ *n=5*). Unpaired Student's t-test.

Figure S2- related to main Figure 2

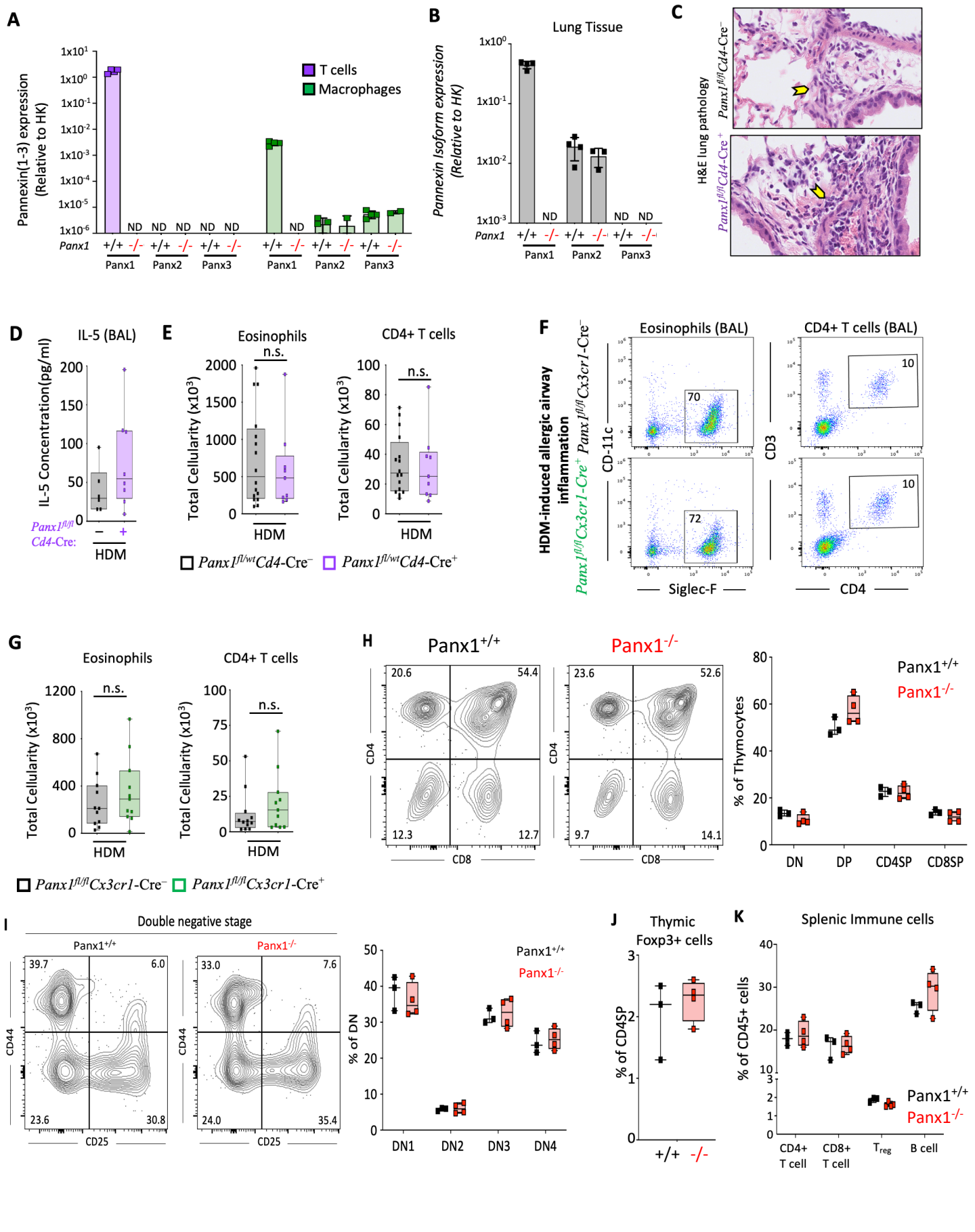

Figure S2, , related to main Figure 2. Panx1 gene expression in different cell types, airway inflammatory phenotype in different Panx1 deleted mice and immune characterization of the Panx1 deficient mice.

(A) Panx1 expression on mouse $CD4^+$ T cells and mouse bone-marrow derived macrophages in wild-type (*n=4*) or *Panx1*$^{-/-}$ (*n=3*) mice via RT-qPCR.

(B) qPCR analysis of *Panx1, Panx2,* and *Panx3* expression in wild type and *Panx1*$^{-/-}$ mice in total lung tissue. (*Panx1*$^{+/+}$ *n=4, Panx1*$^{-/-}$ *n=3*).

(C) Magnified H&E lung histology images of *Panx1*$^{fl/f}$*Cd4-cre*$^{-}$ and *Panx1*$^{fl/f}$*Cd4-cre*$^{+}$ mice from Figure 2C during HDM challenge. Arrows highlight areas of immune cell infiltration and inflammation.

(D) Trending increase in IL-5 in the bronchoalveolar lavage fluid of *Panx1*$^{fl/fl}$ *Cd4-cre*$^{+}$ mice after HDM challenge.

(E) Absolute cellularity of eosinophils (left) and $CD4^+$ T cells (right) in the BAL of Panx1 heterozygous or wild-type mice with or without *Cd4-cre* expression after HDM challenge (*Panx1*$^{fl/wt}$*Cd4-cre*$^{-}$ *n=16, Panx1*$^{fl/wt}$*Cd4-cre*$^{+}$ *n=9*). Unpaired Student's t-test.

(F) Flow plots for eosinophil and $CD4^+$ T cell infiltration into the bronchoalveolar space after HDM challenge in *Panx1*$^{fl/f}$*Cx3cr1-cre* mice.

(G) Absolute cellularity of eosinophils (left) and $CD4^+$ T cells (right). Unpaired Student's t-test (*Panx1*$^{fl/f}$*Cx3cr1-cre*$^{-}$ *n=12, Panx1*$^{fl/f}$*Cx3cr1-cre*$^{+}$ *n=11*).

(H, I) Flow plots (left) and quantification (right) of thymocyte development in *Panx1*$^{+/+}$ and *Panx1*$^{-/-}$ mice. (*Panx1*$^{+/+}$ *n=3, Panx1*$^{-/-}$ *n=4*).

(J) Percentage of thymic Foxp3+ Treg cells in *Panx1*$^{+/+}$ and *Panx1*$^{-/-}$ mice. (*Panx1*$^{+/+}$ *n=3, Panx1*$^{-/-}$ *n=4*).

(K) Percentage of splenic $CD4^+$ T cells, CD8+ T cells, Treg cells, and B cells in *Panx1*$^{+/+}$ and *Panx1*$^{-/-}$ mice. (*Panx1*$^{+/+}$ *n=3, Panx1*$^{-/-}$ *n=4*).

Figure S3- related to main Figure 2

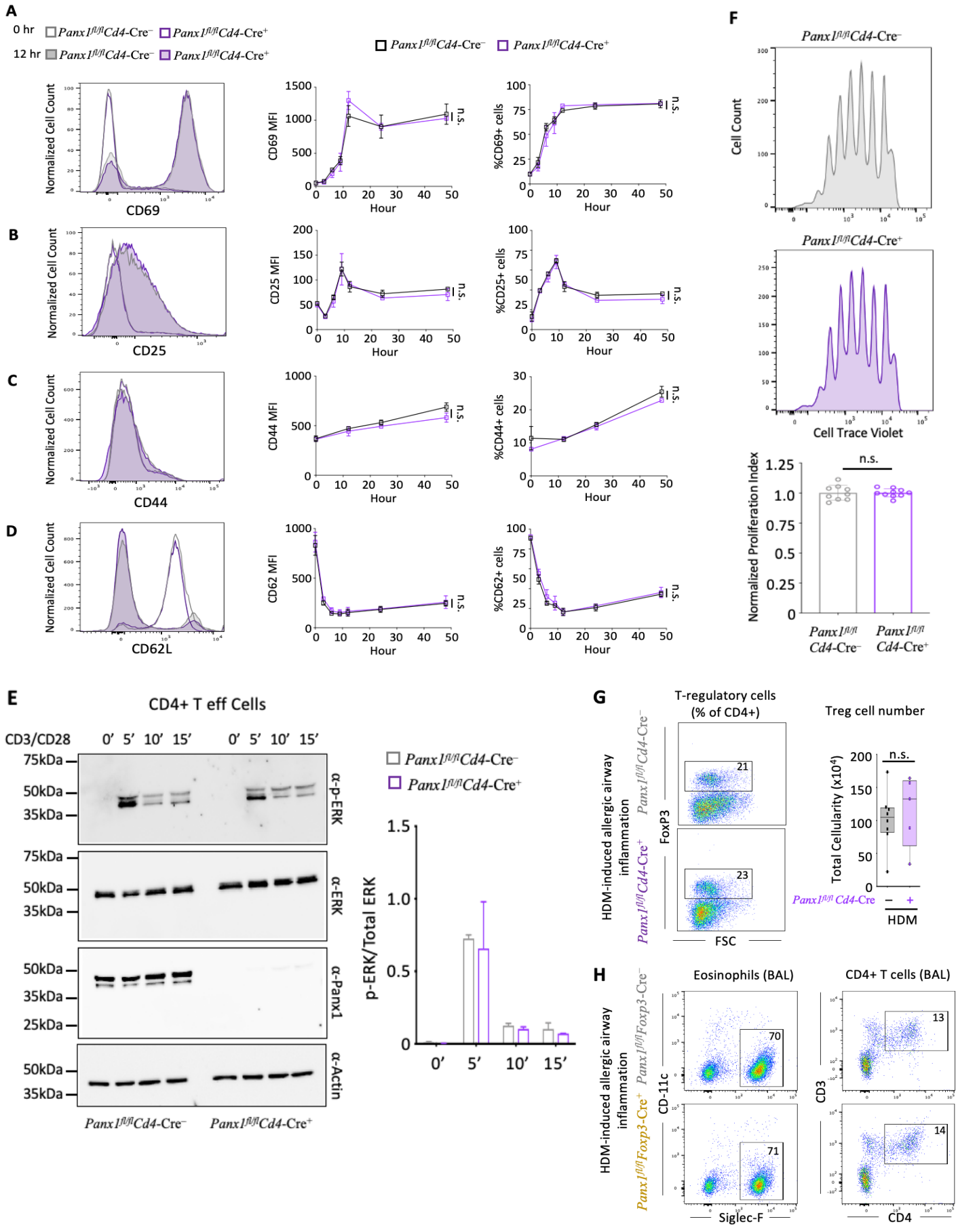

Figure S3, related to main Figure 2. Panx1 deletion does not intrinsically affect T effector cell activation or T regulatory intrinsic function.

(A-D) Time course expression analysis of the activation markers in wild type and *Panx1*$^{-/-}$ CD4^{+} Teff cells (CD4+ CD25-) (right) and flow cytometry histograms at t=0 or t=12 hours after CD3 and CD28 mediated T cell activation (left). (A) CD69; (B) CD25; and (C) CD44, (D) CD62L (which goes down in expression during activation); (n=3). Data are mean ± s.e.m. Analyzed by two-way ANOVA.

(E) Immuno blot time course analysis of downstream TCR signaling via p-ERK in wild-type and *Panx1*$^{-/-}$ CD4^{+} T effector cells (CD4+ CD25-) (left) and quantitative analysis after CD3 and CD28 mediated T cell activation (right).

(F) Histograms of Cell Trace Violet dilution as a measurement of T cell proliferation after CD3 and CD28 mediated activation in wild type and *Panx1*$^{-/-}$ CD4^{+} Teff cells (CD4+ CD25-) (left). Normalized proliferative index between wild-type (*n=9*) and *Panx1*$^{-/-}$ (*n*=10) CD4^{+} T effector cells. Data are mean ± s.d. Unpaired Student's t-test.

(G) (left) Flow plots showing the number of Treg cells in the lung during allergic airway inflammation. (right) Absolute cellularity of Treg cells (*Panx1*$^{fl/fl}$*Cd4-cre*$^{-}$ *n=8, Panx1*$^{fl/fl}$*Cd4-cre*$^{+}$ *n=5*). Unpaired Student's t-test.

(H) Flow plots showing eosinophil and CD4^{+} T cell infiltration into the bronchoalveolar space after HDM challenge in *Panx1*$^{fl/fl}$*Foxp3-cre*$^{-}$ and *Panx1*$^{fl/fl}$*Foxp3-cre*$^{+}$ mice.

Figure S4- related to main Figure 3

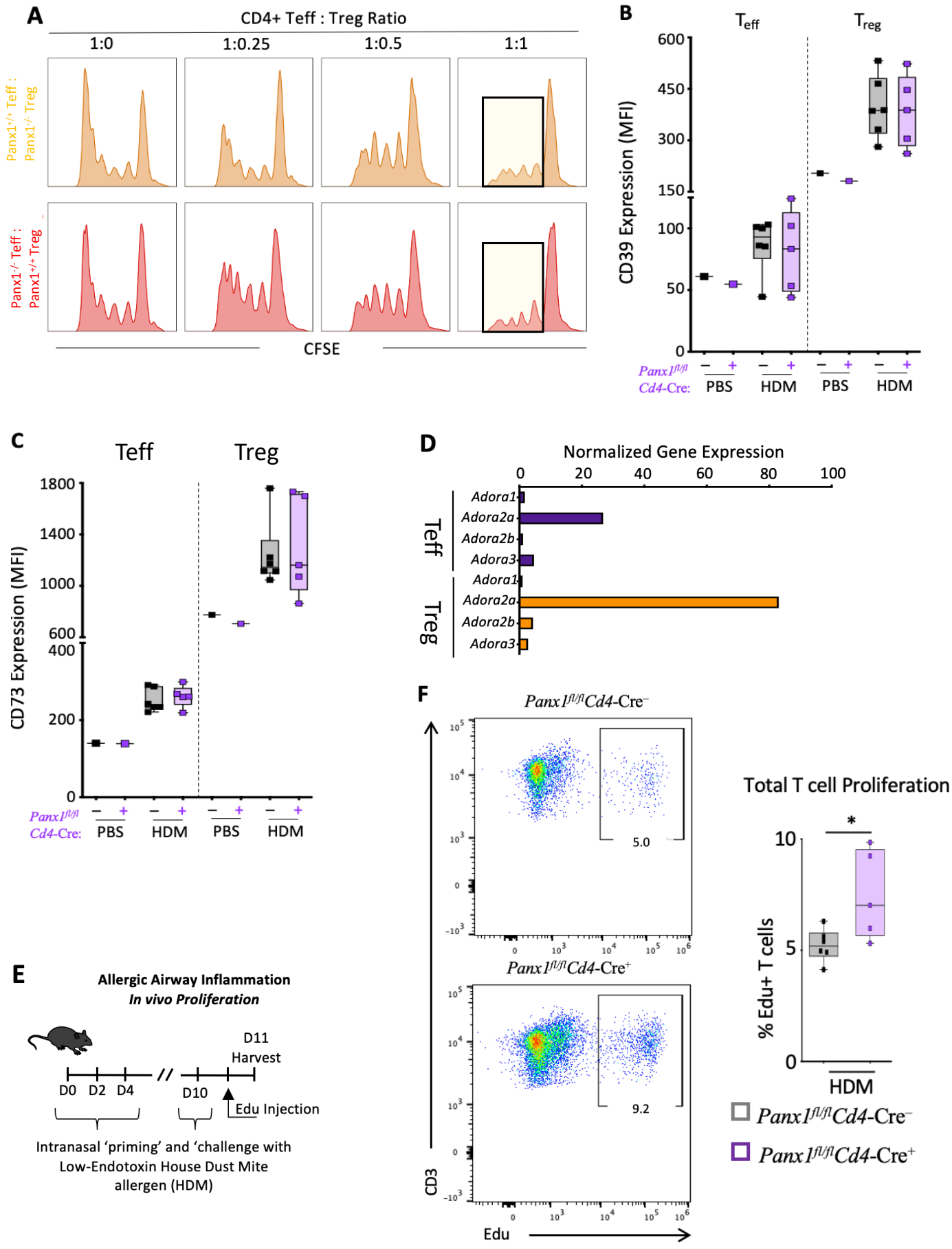

Figure S4, related to main Figure 3. Panx1 intercellular functions during T cell proliferation and characterization of important extracellular nucleotide molecules.

(A) Histograms of combinatorial suppression assays with wild type and *Panx1*$^{-/-}$ Teff and Treg cells at indicated cell ratios.

(B) MFI quantification of CD39 in *Panx1*$^{fl/fl}$*Cd4-cre* mice. (*Panx1*$^{fl/f}$*Cd4-cre*$^{-}$ *n=6, Panx1*$^{fl/f}$*Cd4-cre*$^{+}$ *n=5*).

(C) MFI quantification of CD73 in *Panx1*$^{fl/fl}$*Cd4-cre* mice. (*Panx1*$^{fl/f}$*Cd4-cre*$^{-}$ *n=6, Panx1*$^{fl/f}$*Cd4-cre*$^{+}$ *n=5*).

(D) Gene expression data from the Immgen database assessing the relative expression of Adenosine Receptors in Teff and Treg cells.

(E) Schematic representation for the modified mouse model of house dust mice induced allergic airway inflammation to measure T cell proliferation *in vivo*.

(F) Quantitative analysis of total CD3^{+} EdU+ T cells in *Panx1*$^{fl/f}$*Cd4-cre*$^{-}$ (*n=6)* and *Panx1*$^{fl/f}$*Cd4-cre*$^{+}$ (*n=5)* mice during HDM. Unpaired Student's t-test.

Figure S5- related to main Figure 4

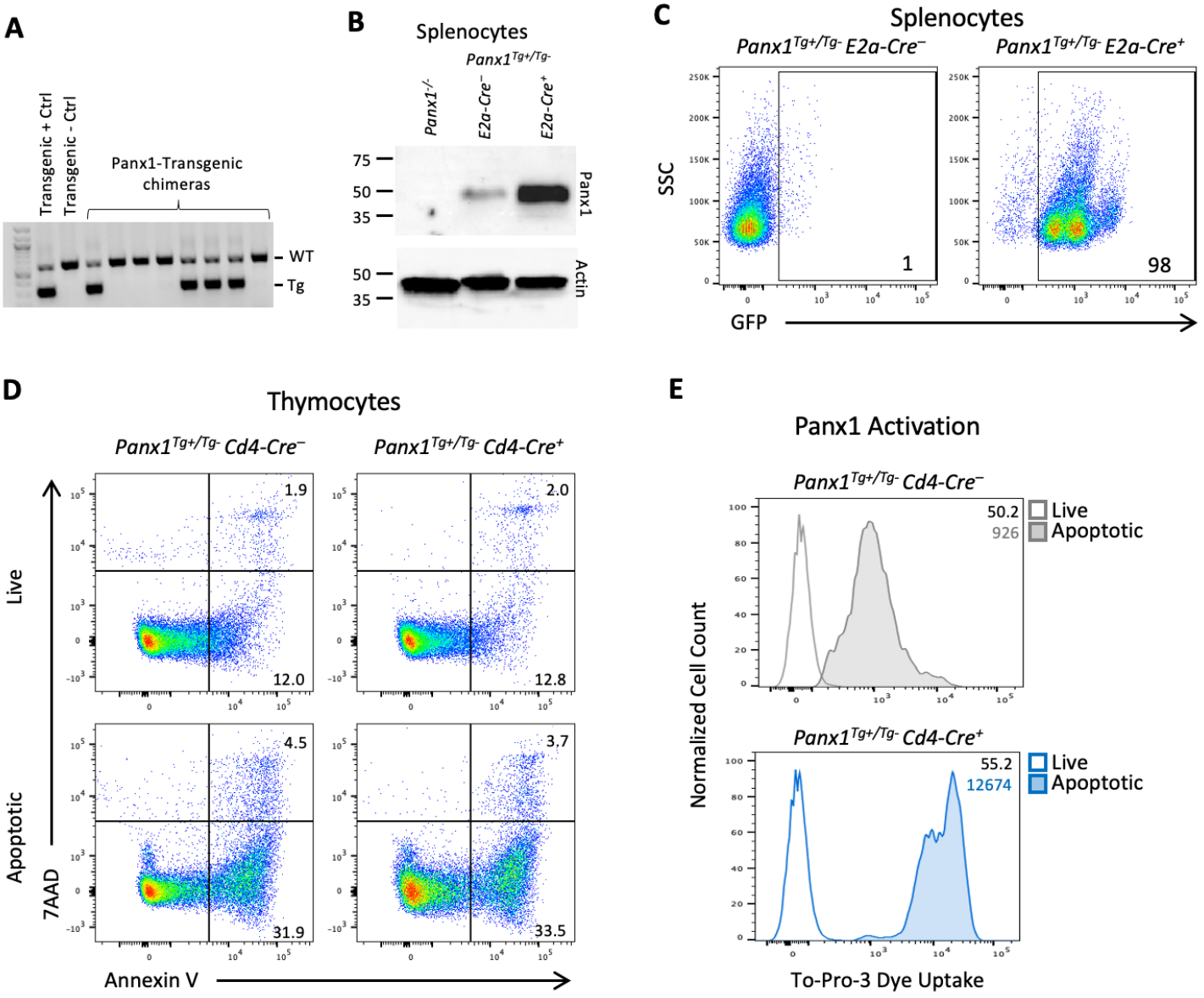

Figure S5, related to main Figure 4. Generation and validation of *Panx1^{Tg}* mice.

(A) PCR analysis of *Panx1^{Tg}* chimeric mouse genomic DNA to ensure proper integration of the transgene into the *ROSA-26* locus.

(B) Immuno blot validation of Panx1 over-expression in mice by crossing the *Panx1^{Tg}* mice to *E2a-cre* mice and assessing Panx1 protein in the spleen. Actin expression was used as a loading control.

(C) Validation of eGFP expression in splenocytes from *Panx1^{Tg} E2a-cre* or wild type control mice.

(D) Functional analysis of transgenic Panx1 by TO-PRO-3 dye uptake during apoptosis. *Panx1^{Tg} Cd4-cre^{+}* and control *Panx1^{Tg} Cd4-cre^{-}* thymocytes were analyzed for apoptosis induction via annexin V and 7AAD staining, and both showed comparable cell death.

(E) Histograms and MFI of TO-PRO-3 dye uptake within apoptotic cells of respective mice.

Figure S6- related to main Figure 5 and 6

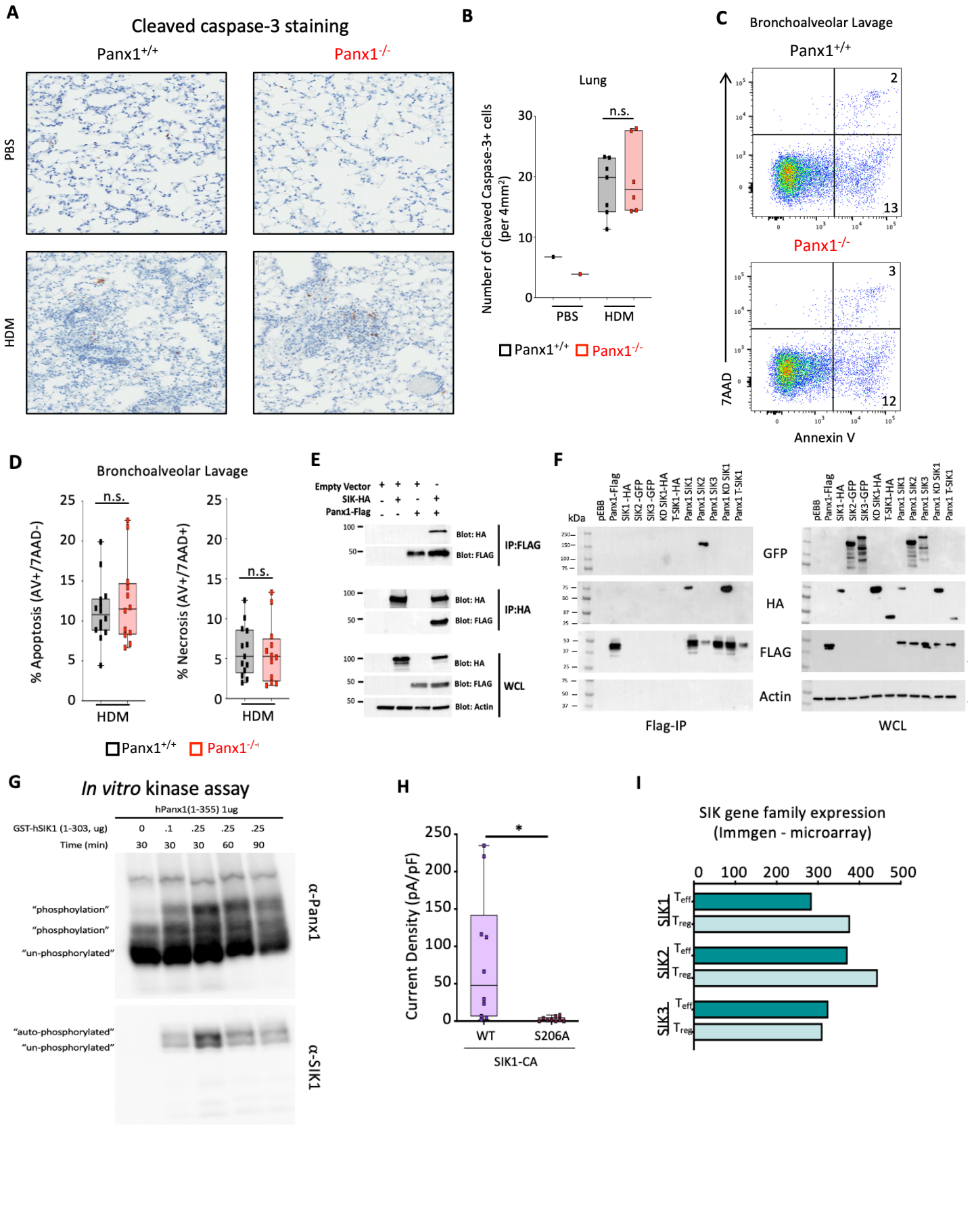

Figure S6, related to main Figure 5 and 6. Panx1 function during airway inflammation is independent of caspases, but relies on SIK family kinases for channel activation.

(A) Cleaved caspase-3 staining in lungs of wild-type and global *Panx1*$^{-/-}$ mice during HDM challenge or control PBS.

(B) Quantitation of the number of cleaved caspase-3 positive cells in wild-type and global *Panx1*$^{-/-}$ lungs (PBS–*Panx1*$^{+/+}$ *n=1,* PBS–*Panx1*$^{-/-}$ *n=1,* HDM–*Panx1*$^{+/+}$ *n=8,* HDM–*Panx1*$^{-/-}$ *n=6*). Unpaired Student's t-test.

(C) Flow cytometry plots assessing the extend of cell death (using Annexin V and 7AAD) in the BALF from wild-type and global *Panx1*$^{-/-}$ mice.

(D) Quantitative analysis of apoptosis (left, only annexin V positive) and secondarily necrotic (right, annexin V and 7AAD positive)) in wild-type and *Panx1*$^{-/-}$ BALF (HDM–*Panx1*$^{+/+}$ *n=14,* HDM–*Pan1*$^{-/-}$ *n=12*). Unpaired Student's t-test.

(E) Immuno blot analysis of co-immunoprecipitations with Panx1-Flag, SIK-HA, or empty vector control in HEK293T cells. Actin was used as a whole cell lysate loading (WCL) control.

(F) Immuno blot analysis of co-immunoprecipitations with Panx1-Flag, SIK-HA, SIK2-GFP, SIK3-GFP, SIK1-kinase dead (KD), SIK1-truncated(T) or empty-vector control in HEK293T cells. Actin was used as a whole cell lysate loading (WCL) control.

(G) Phos-tag SDS page gel analysis of *in vitro* kinase assays using purified recombinant hPanx1 (1-355) and recombinant hSIK1(1-303) incubated at different concentrations and timepoints. A cleaved form of Panx1 was used for higher purification quality and the commercially purchased cleaved SIK1 is 'constitutively active'.

(H) Current density quantification from whole cell patch-clamp recordings of Panx1 currents in HEK293T cells transfected with SIK1-CA and either hPANX1-WT or hPANX1-S206A (*p <0.01). Unpaired Student's t-test.

(I) Gene expression data from the Immgen database assessing the relative expression of *SIK1, SIK2,* and *SIK3* in Teff and Treg cells.